Improvement of QDIP performance due to quantum dots with built-in charge

Vladimir Mitin [a,*], Andrei Sergeev [a], Nizami Vagidov [b], Stefan Birner [c]

[a] University at Buffalo, The State University of New York, Buffalo, NY 14260, USA
[b] Optoelectronic Nanodevices LLC, Amherst, NY 14226, USA
[c] Walter Schottky Institut and Physics Department, Technische Universitat München, D-85748 Garching, Germany

ARTICLE INFO

ABSTRACT

The charging of quantum dots provides two strong effects which improve Quantum Dot Infrared Photodetector (QDIP) performance. First, electrons placed in the quantum dots enhance IR-induced transitions and increase electron coupling to IR radiation. Second, the built-in-dot charge creates potential barriers around dots and these barriers strongly suppress the photoelectron capture and exponentially increase the photoelectron lifetime. Both effects enhance the IR photoresponse. Long photoelectron lifetime decreases the generation–recombination noise and increases the device sensitivity. To investigate the potential profiles around charged dots, we used the nextnano3 software which allows for simulation of multilayer structures combined with realistic geometries in one, two, and three spatial dimensions. In weak electric fields the photoelectron kinetics and transport in the potential created by charged dots have been studied analytically. In strong fields the results were based on Monte-Carlo modeling. The effects of dot charging have been investigated in QD structures which were fabricated using molecular beam epitaxy. InAs quantum dots were grown on AlGaAs surfaces by deposition of approximately 2.1 monolayers of InAs. In the obtained structures the dot charging is realized via intra-dot and inter-dot doping. The increase in photoresponse due to dot charging is in good agreement with the model which takes into account anisotropy of potential barriers around QDs in QD layers.

Published by Elsevier B.V.

1. Introduction

Quantum-Well Infrared Photodetector (QWIP) which is currently used in imaging devices demonstrates the detectivity of about 10^{10} cm Hz$^{1/2}$/W when operating at $T = 77$ K around $\lambda = 10$ μm. At room temperature its detectivity drops almost by two orders of magnitude. This high-temperature limitation is caused by radical decrease of the photoelectron lifetime which defines the operation of infrared photodetectors. The decrease in photoelectron lifetime reduces the detector's responsivity and sensitivity [1–6].

Compared with quantum-well structures, quantum-dot materials provide more possibilities for managing photoelectron lifetime and other optoelectronic characteristics via manipulation of electron processes in dots [1,7], band engineering [8,9], etc. Our original approach [10–13] is based on the management of photoelectron kinetics via engineering of the nanoscale potential profile by using charged quantum dots. Charging of quantum dots may be realized by selective doping of the QD media. Various vertical and lateral alignments of charged QDs or dot clusters allow

one to obtain very specific potential profiles with high potential barriers that separate QDs from conducting channels where electron transport takes place. By separating mobile photoelectrons from QDs by the potential barriers (see Fig. 1) we suppress the photoelectron capture processes and increase the lifetime of photoelectrons.

2. Effect of barriers on the photoelectron lifetime and QDIP performance

The photoelectron capture by the repulsive charged QD may be realized via tunneling through the surrounding barrier or thermal excitation above the barrier. Relative probability of these processes is determined by the radius of a quantum dot, a. Our evaluations show [11] that, if the radius is greater than 5 nm, the thermally activated processes dominate over the tunneling processes, and the electron capture rate, $1/\tau_{cap}$, is expected to follow the exponential dependence:

$$\frac{1}{\tau_{cap}} = \pi N_{dot} a^3 \tau_\varepsilon^{-1} \exp\left(-\frac{V_h}{k_B T}\right), \tag{1}$$

where N_{dot} is the dot concentration, a is the quantum dot radius, V_h is the height of the potential barrier around the dot, and τ_ε is the

---

* Corresponding author.
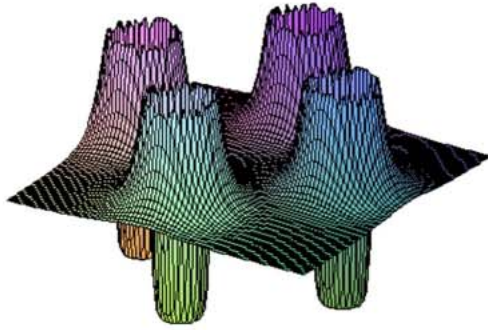 *E-mail address:* vmitin@buffalo.edu (V. Mitin).

Fig. 1. Potential barriers around spherical quantum dots.

electron–phonon relaxation time which corresponds to transitions from conducting states to the localized QD states. Thus, the electron lifetime with respect to the capture by n-charged QDs exponentially depends on the height of the potential barriers which itself are a function of the built-in-dot charge.

The increase in photoelectron lifetime (Eq. (1)) directly improves the photoconductive gain,

$$g = \frac{\tau_{cap}}{\tau_{tr}}, \tag{2}$$

where τ_{cap} is the photoelectron lifetime and τ_{tr} is the transport time which electron spends in the sensor before leaving it through the contacts, i.e. $\tau_{tr} = d/\mu E$, where d is the length of a sensor and μ is the mobility of photoelectrons in the sensor. The photoconductive gain increases the responsivity of the detector,

$$R = \frac{e}{h\nu}\eta g \tag{3}$$

where η is the quantum efficiency of photoelectron generation process which includes both the absorption efficiency and intrinsic efficiency.The noise of the photodetector is equal to the background noise when photodetector is operating in the regime of the background limited performance (BLIP). The average fluctuation of the background radiation is given by: $\eta_0(\Phi_{BG}S)^{1/2}$, where S is the absorption area of the photodetector, Φ_{BG} is the background photon flux density, and η_0 is the absorption coefficient.The fluctuation in the photogeneration rate can be expressed through an intrinsic quantum efficiency, η_i, which is defined as the probability of carrier generation by an absorbed photon. Then, the fluctuation of the background radiation can be expressed as: $\eta_i\eta_0(\Phi_{BG}S)^{1/2}$

Kinetics of the thermal carriers defines the intrinsic generation–recombination noise. The generation rate can be defined as: $n_{th}V/\tau_{cap}$ and its average fluctuation as: $(n_{th}V/\tau_{cap})^{1/2}$, near thermodynamic equilibrium. Here V is the volume of the photodetector, n_{th} is the thermal carrier concentration, and τ_{cap} is the carrier lifetime. The thermal generation noise, under the BLIP regime, should be as low as the photogeneration noise due to background fluctuations:

$$\sqrt{\frac{n_{th}V}{\tau_{cap}}} = \eta_0\eta_i\sqrt{\Phi_{BG}S} \tag{4}$$

and therefore:

$$\Phi_{BLIP} = \frac{n_{th}d}{(\eta_0\eta_i)^2\tau_{cap}} \equiv G_{th} \tag{5}$$

where $d = V/S$ is the length of the detector.

The sensitivity of the detector is described in terms of the noise equivalent power (NEP), which is defined as an equivalent fluctuation of the background radiation power:

$$NEP_{GR} = \frac{h\nu}{\eta}\sqrt{\frac{2n_{th}V}{\tau_{cap}}} = h\nu\sqrt{2SG_{th}} \tag{6}$$

where $\eta = \eta_0\eta_i$. The corresponding detectivity of the sensor is given by:

$$D^* = \frac{\sqrt{S}}{NEP_{GR}} = \frac{\eta}{h\nu}\sqrt{\frac{\tau_{cap}}{2n_{th}d}} \tag{7}$$

Thus, the charging of quantum dots exponentially increases the photoelectron lifetime (Eq. (1)) and linearly increases the absorption coefficient, η_0. Both these factors improve the responsivity of the detector (Eq. (3)). The increase in the photoelectron lifetime also suppresses the generation–recombination noise. Finally, the sensivity of the detector, i.e. NEP_{GR} or the detectivity (Eqs. (6) and (7)), is significantly improved by the dot charging due to the increase of photoelectron lifetime and absorption coefficient.

The above analysis based on the increase of photoelectron lifetime (Eq. (1)) is valid for weak electric fields when the nonequilibrium distribution function averaged over the electron momentum directions is small. For high electric fields we employ the Monte-Carlo modeling [14]. The developed Monte-Carlo program includes all basic scattering processes, including electron scattering on acoustic, polar optical, and intervalley phonons. The electron transport is considered in three valleys: Γ, L, and X. The redistribution of carriers between these valleys as a result of electron heating by electric field is taken into account. To simplify the model of simulations we assume that the dots of radius a are arranged in a regular lattice pattern with the inter-dot distance of d_{id}. The dot concentration N_{dot} is defined as $1/d_{id}^3$. In our model, we consider the carrier capture process as an electron–phonon relaxation process: (i) which is limited in space by the dot volume and (ii) during which a carrier transits from a conducting state above the potential barrier to a localized (bound) state which is below the potential barrier. In other words, we assume that from the bound state a carrier relaxes to deeper dot states faster than it could return back to the conducting state.

On the basis of the Monte-Carlo modeling we calculated the dependence of the electron capture time, τ_{cap}, on the electric field at different maximum values of the potential barrier. The results of simulation show that the capture time is practically independent on the electric field up to the critical field of the order of 10^3 V/cm. At electric fields higher than the critical field, the electron capture time, τ_{cap}, radically decreases with the field increase (see Fig. 2).

The effect of the electric field on the photoelectron lifetime may be understood in terms of the electron heating. The electric field increases the electron temperature and, when the temperature shift becomes comparable with the height of potential barriers
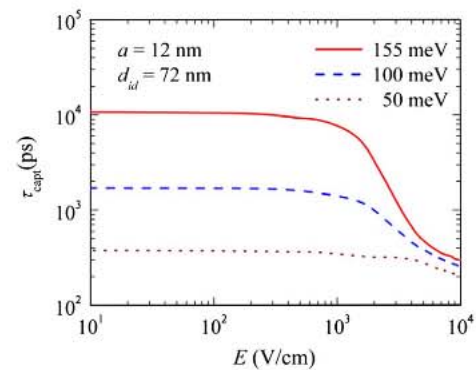

Fig. 2. Capture time as a function of the electric field for different heights of potential barriers: 155, 100, and 50 meV, respectively.
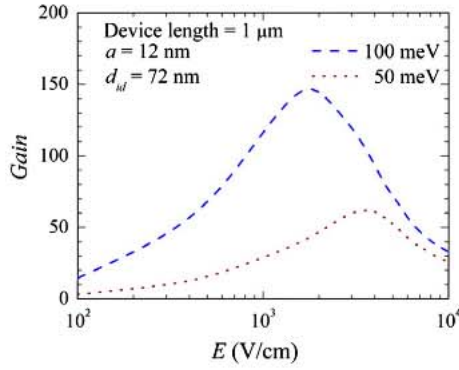
Fig. 3. Photoconductive gain as a function of the electric field.

Table 1
Parameters of B44, B45, B52, and B53 QDIPs.

Device	B44	B45	B52	B53
Intra- and inter-dot doping	Intra	Inter	Intra	Inter
Donor concentration (10^{11} cm^{-2})	2.7	2.7	5.4	5.4
Number of electrons in dot, n	2.7	2.8	4.7	6.1
Built-in-dot charge, n_q	1.8	2.8	3.45	6.1

around dots, the hot electrons overcome the barriers and are captured by the dots via electron–phonon relaxation processes. Therefore, the photoconductive gain is expected to have non-monotonic dependence on the electric field with the maximum slightly above the characteristic field of $\sim 10^3$ V/cm (see Fig. 3). At weak electric fields the gain increases due to the increase of the drift velocity, $v_d = \mu E$ and the corresponding decrease of the transit time, $\tau_{tr} = d/v_d$. Above the critical field that provides electron overheating large enough for overcoming the potential barriers the photoelectron lifetime exponentially decreases with the electron temperature.

3. Enhancement of photoresponse due to built-in-dot charge

The quantum-dot photodetector structures were grown by molecular beam epitaxy (MBE) on n$^+$-GaAs (100) substrate. The QDs were distributed over QD layers randomly. The average distance between QDs was 31 nm which corresponds to the sheet concentration of dots $\sim 10^{11}$ cm^{-2}. Details of fabrication technique and parameters of the investigated devices can be found elsewhere [12,13]. The structures consisted of 10 layers of InAs QDs with a lateral size of 15 nm and average height of 3.6 nm spaced by a 50 nm thick Al$_{0.22}$Ga$_{0.78}$As layer. The AlGaAs spacer layer was chosen wide in order to dissipate strain accumulation from one layer to the next.

Two methods of doping of the investigated devices were chosen: intra-dot doping (devices B44 and B52, see Fig. 4a) and inter-dot doping (devices B45 and B53, see Fig. 4b). Samples B44, B45 and B52, B53 had donor sheet concentrations 2.7×10^{11} cm^{-2} and 5.4×10^{11} cm^{-2}, respectively. In B44 and B52 quantum dot layers were homogeneously doped, while in B45 and B53 only the middle of each AlGaAs barrier layer was δ-doped. The parameters of these devices are given in Table 1.

The bandstructure and potential distribution of real devices were found by using nextnano3 software [15]. This simulation tool allows taking into account strain in multilayer heterostructures and self-consistently solves Schrödinger, Poisson, and current equations. The profiles of conduction and valence bands can be calculated either within single-band or multi-band $k \cdot p$ models. The variations of the built-in-dot charge and potential profile in two orthogonal to each other directions are shown in Fig. 5. This figure clearly shows the channels between quantum dots where electron transport takes place.

Note, that the potential barriers around QDs are strongly asymmetric: the barriers along the quantum dot layers (in the C–D-direction which is perpendicular to the current) are substantially smaller than the barriers in the direction of the current (A–B-direction). This asymmetry has strong consequences for the kinetics of photocarriers. The electron trapping is more effective for electrons moving along the C–D-direction than for electrons moving in A–B-direction. Therefore, the capture processes in QD planes will dominate in the relaxation processes [16]. The dependence of the barrier height, which is found from Fig. 5, on the built-in-dot charge can be described as:

$$V_{C-D} = bn_q \qquad (8)$$

with $b = 2.5$ meV. It is obvious that in the case of the intra-dot doping, the dot charge n_q is equal to the dot population, n, reduced by
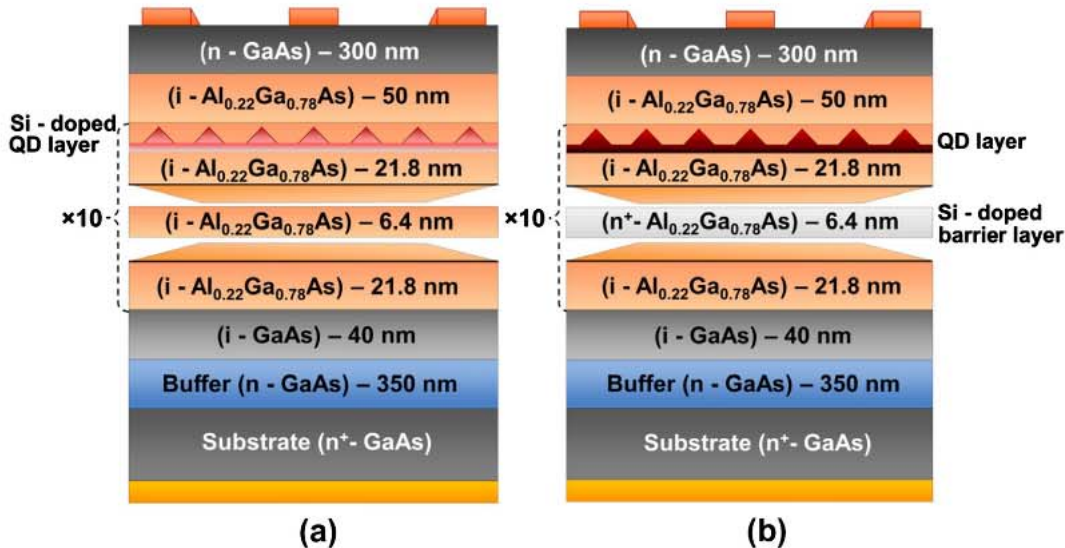

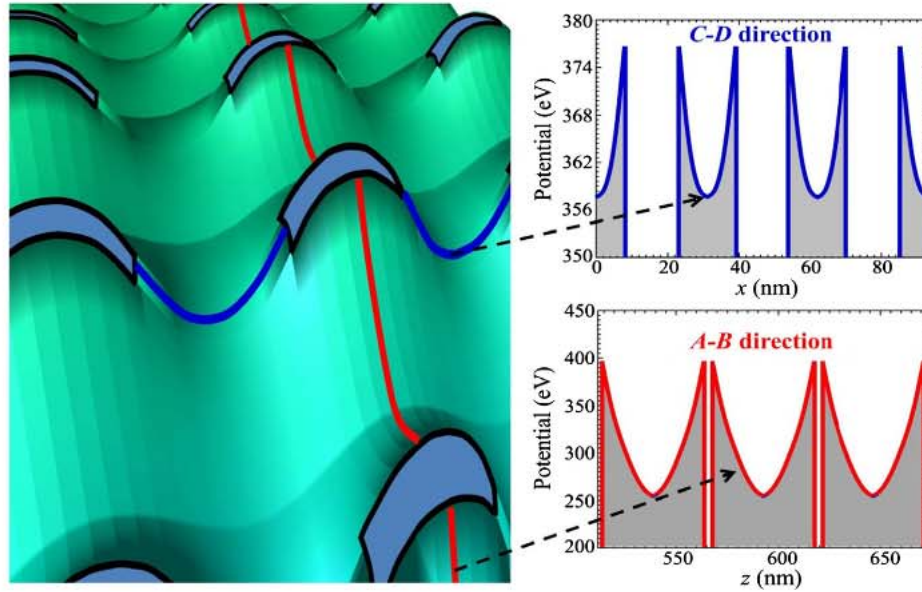Fig. 4. Schematics of two quantum-dot photodetectors with intra-dot (a) and inter-dot (b) doping.

Fig. 5. Three-dimensional potential profile of QDIP with cross-sections in *A–B* and *C–D* directions.

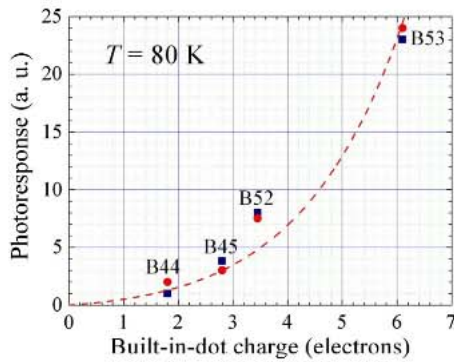**Fig. 6.** The photocurrent as a function of the built-in-dot charge. The blue squares are for experimental data ($\lambda = 3.77$ μm) and the red circles are for modeling results. The red dashed line is the theoretical dependence for the inter-dot doping. (For interpretation of the references to colour in this figure legend, the reader is referred to the web version of this article.)

Fig. 7. Calculated detectivity of samples B44, B45, B52, and B53 ($\lambda = 3.77$ μm) as a function of the built-in-dot charge. The blue solid line is the universal dependence for QDIPS with inter-dot doping of QD medium. (For interpretation of the references to colour in this figure legend, the reader is referred to the web version of this article.)

the number of dopants, p, in the dot, i.e. $n_q = n-p$. In the case of the inter-dot doping, the built-in-dot charge, Q, is equal to en. Taking into account these considerations, the effects of doping on the photocurrent in QDIPs can described as:

$$I = An \exp\left(-\frac{bn_q}{k_B T}\right) \qquad (9)$$

In the last equation, A is an arbitrary constant which does not depend on doping. The pre-exponential factor in Eq. (9) describes the increase of the absorption with the increase of electron filling of the dot, n. The exponential factor describes the influence of QD potential barrier height on the photoelectron lifetime. The height of the potential barrier created around QDs is proportional to the built-in-dot charge which is defined by the number of electrons and number of dopants in the dot.

In the framework of the described model of capture processes in QD layers the experimental data can be fitted as it is shown in Fig. 6 where we used the values of n, determined from self-consistent modeling (see Table 1). As seen, the theoretical modeling (red circles) is in a very good agreement with experimental data (blue
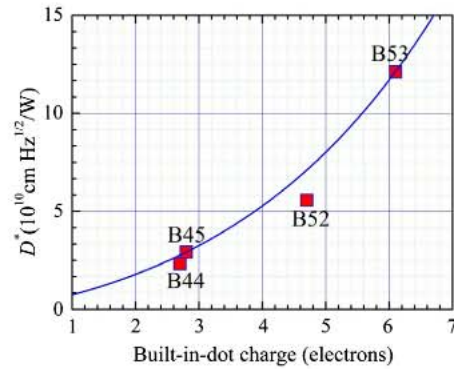
squares). From this fitting, the parameter b was found to be equal to 2.7 meV, which is in very good agreement with $b = 2.5$ meV that we obtained from the independent modeling of the potential barrier heights. The red dashed line shows the modeling results for the inter-dot doping ($n = n_q$), which was used for samples B45 and B53. For samples B44 and B52 with the homogeneous doping of QD layers, the dot charge was created by the electrons captured in the dot and dopants placed in the dot. In this case, $n = n_q + p$ and the corresponding red circles lie above the dashed line.

As seen, the proposed, relatively simple model provides very good description of doping effects on the photoresponse of QD structures. We believe that such good agreement with experiment evidences that the model adequately takes into account the main effects of doping on photoelectron kinetics.

The presented in Fig. 7 detectivity was calculated using Eq. (7). The concentration of the thermally excited electrons, n_{th}, determined from the dark current measurements, was equal to 10^8 cm^{-3}. Conservative estimates for the structure with one electron per dot give the absorption coefficient equal to $\eta = 1\%$ and the photoelectron capture time equal to $\tau_{cap} = 10$ ps. The increase of QD charging is expected to improve the detectivity because of

the increase of electron coupling to radiation and increase of photoelectron lifetime.

4. Conclusions

Our new approach, based on engineering of three-dimensional potential barriers introduced by quantum dots with built-in-dot charge, provides real opportunities to radically improve the performance of IR photodetectors [17]. Novel design methodology has a number of attractive features:

- Significant suppression of recombination processes due to the built-in-dot charge which creates the potential barriers around QDs and QD clusters.
- Strong harvesting and conversion of IR radiation via QD electron transitions that are enhanced by the built-in-dot charge.
- Effective management of the photoelectron kinetics and generation–recombination processes by the built-in-dot charge.
- Strong potential for adaptive sensing via control of the built-in-dot charge by bias and/or gate voltage.
- This approach does not require electron inter-dot coupling that leads to substantial limitations on fabrication of corresponding QDIPs.

Modern technologies allow for fabrication of specific structures with various combinations of quantum dots, dot clusters, and other nanoblocks of QDs, conducting channels, and barriers between blocks and channels. This provides numerous possibilities for engineering very specific 3D barriers. We believe that in future electronic and sensing technologies, the 3D barriers will be employed in every device, as nowadays technology employs semiconductor heterostructures with 1D barriers.

Acknowledgments

References

[1] E.A. Zibik, T. Grange, B.A. Carpenter, N.E. Porter, N. Ferreira, G. Bastard, D. Stehr, S. Winnerl, M. Helm, N.Y. Liu, M.S. Skolnick, L.R. Wilson, Long lifetimes of quantum-dot intersublevel transitions in the terahertz range, Nat. Mater. 8 (2009) 803–807.
[2] M. Razeghi, H. Lim, S. Tsao, J. Szafraniec, W. Zhang, K. Mi, B. Movaghar, Transport and photodetection in self-assembled semiconductor quantum dots, Nanotechnology 16 (2005) 219–229.
[3] J.C. Campbell, A. Madhukar, Quantum dot infrared detectors, IEEE Quant. Electron. 95 (2007) 1815–1827.
[4] A.V. Barve, S.J. Lee, S.K. Noh, S. Krishna, Review of current progress in quantum dot infrared photodetectors, Laser and Photonics Reviews (2009) 1–17.
[5] B.F. Levine, Quantum-well infrared photodetectors, J. Appl. Phys. 74 (1993) R1–R79.
[6] S.D. Gunapala, S.V. Bandara, J.K. Liu, C.J. Hill, S.B. Rafol, J.M. Mumolo, J.T. Trinh, M.Z. Tidrow, P.D. LeVan, 1024×1024 pixel mid-wavelength and long-wavelength infrared QWIP focal plane arrays for imaging applications, Semicond. Sci. Technol. 20 (2005) 473–480.
[7] V. Ryzhii, The theory of quantum-dot infrared phototransistors, Semicond. Sci. Technol. 11 (2005) 759–765.
[8] A. Luque, A. Marti, The intermediate band solar cell: progress toward the realization of an attractive concept, Adv. Mater. 22 (2010) 160–174.
[9] S. Tomic, Intermediate-band solar cells: influence of band formation on dynamical processes in InAs/GaAs quantum dot arrays, Phys. Rev. B 82 (2010) 195321-1–195321-15.
[10] V.V. Mitin, V.I. Pipa, A.V. Sergeev, M. Dutta, M. Stroscio, High-gain quantum-dot infrared photodetector, Infrared Phys. Technol. 42 (2001) 467–472.
[11] A. Sergeev, V. Mitin, M. Stroscio, Quantum-dot photodetector operating at room temperatures: diffusion-limited capture, Physica B 316–317 (2002) 369–372.
[12] K.A. Sablon, J.W. Little, V. Mitin, A. Sergeev, N. Vagidov, K. Reinhardt, Strong enhancement of solar cell efficiency due to quantum dots with built-in charge, Nano Lett. 11 (2011) 2311–2317.
[13] V. Mitin, A. Antipov, A. Sergeev, N. Vagidov, D. Eason, G. Strasser, Quantum dot infrared photodetectors: photoresponse enhancement due to potential barriers, Nanoscale Res. Lett. 6 (2011) 21-1–21-6.
[14] V. Mitin, A. Sergeev, L-H. Chien, N. Vagidov, Monte-Carlo modeling of electron kinetics in room temperature quantum-dot photodetectors, in: I. Lirkov, S. Margenov (Eds.), Large-Scale Scientific Computing, Springer, Berlin, Heidelberg, 2010, pp. 403–410.
[15] http://www.nextnano.de/nextnano3.
[16] K. Sablon, A. Sergeev, N. Vagidov, A. Antipov, J.W. Little, V. Mitin, Effective harvesting detection, and conversion of IR radiation due to quantum dots with built-in charge, Nanoscale Res. Lett. 6 (2011). 584-1-13.
[17] A. Sergeev, L-H. Chien, N. Vagidov, V. Mitin, Quantum-dot infrared photodetectors: in search of right design for room-temperature operation, in: S. Luryi, J. Xu, A. Zaslavsky (Eds.), Future Trends in Microelectronics: From Nanophotonics to Sensors to Energy, Wiley IEEE Press, 2010, pp. 385–393.